GEOPHYSICAL RESEARCH LETTERS, VOL. 40, 2679–2683, doi:10.1002/grl.50517, 2013

Energy budget of first-year Arctic sea ice in advanced stages of melt

Stephen R. Hudson,[1] Mats A. Granskog,[1] Arild Sundfjord,[1] Achim Randelhoff,[1]
Angelika H. H. Renner,[1] and Dmitry V. Divine[1]

Received 27 March 2013; revised 28 April 2013; accepted 29 April 2013; published 7 June 2013.

[1] During an 8 day drift in July–August 2012 in the Nansen Basin, all components of the energy budget of melting first-year sea ice were observed. Absorption of solar radiation by the ice and ponds was the largest source of energy to the ice at almost all times during the drift. However, oceanic heat flux also provided significant heating and dominated during one wind event. Longwave fluxes provided a relatively small cooling effect, and atmospheric heat fluxes were negligible. The aggregate scale albedo of this younger, thinner ice was significantly lower than at Surface Heat Budget of the Arctic Ocean (SHEBA), and the transmittance was significantly higher here, despite similar pond and open water fractions. The oceanic heat flux was only half of the solar flux through the ice to the water, producing warm water near the surface that might delay ice growth in autumn, an important effect of the transition to thinner first-year ice in the high Arctic. **Citation:** Hudson, S. R., M. A. Granskog, A. Sundfjord, A. Randelhoff, A. H. H. Renner, and D. V. Divine (2013), Energy budget of first-year Arctic sea ice in advanced stages of melt, *Geophys. Res. Lett.*, *40*, 2679–2683, doi:10.1002/grl.50517.

1. Introduction

[2] There has been a well-documented regime shift in the Arctic sea ice cover over the last decade. Summer sea ice extent has decreased drastically, while the winter ice extent maximum has experienced smaller decreases [*Stroeve et al.*, 2012]. The summer melt season has also become longer [*Markus et al.*, 2009]. The result has been a shift over much of the Arctic basin from thick perennial multiyear ice (MYI) to an increasingly seasonal sea ice cover, with younger, thinner first- and second-year ice [*Maslanik et al.*, 2011; *Comiso*, 2012]. A significant decrease in Arctic sea ice thickness and volume has also been established [*Laxon et al*., 2013; *Haas et al*., 2008; *Giles et al*., 2008].

[3] Much of our understanding of Arctic sea ice thermodynamics and mass balance, and therefore their representation in models, stems from observations of thicker MYI. The properties of first-year ice (FYI) are thought to differ significantly from those of MYI, creating potentially significant errors in model simulations. Established differences in the Arctic include higher melt pond coverage, lower surface albedo, increased transmittance of solar radiation into the ocean, and fewer, steeper, and shallower pressure ridges for FYI [e.g., *Frey et al*., 2011; *Polashenski et al*., 2012; *Perovich and Polashenski*, 2012; *Nicolaus et al*., 2012; *Wadhams and Toberg*, 2012]. Thus far, studies of the energy budget of the new thin high-Arctic ice pack have examined individual components of the budget at different times and locations, leaving gaps in the overall picture for any specific location or time of year.

[4] In this paper, we examine simultaneous observations of all components of the energy budget of a high-Arctic (82°N) first-year sea ice pack during advanced melt, identifying the contributions of the atmosphere, ocean, and radiation to ice melt. Using observations of the turbulent energy exchange at the atmosphere-ice and ice-ocean boundaries, along with observations of the radiative fluxes (albedo and transmission through the ice), and accounting for the significant spatial variability of the albedo and transmittance, we present a full picture of the sea-ice energy budget at a large scale for this thinner Arctic sea ice pack.

2. Observations

[5] We conducted our observations during an 8 day ice station (26 July to 3 August 2012) in the drift ice north of Svalbard during the ICE12 expedition on R/V *Lance*, in the southwestern Nansen Basin (82.25°N, 21°E; see supplemental material, Figure S1, for a map). The ice floe had a mean thickness of 0.8 m, generally with 0.3–0.6 m of ice below the dark ponds and 0.8–1.0 m below bright ponds. Based on airborne surveys of ice thickness and aerial photography, the floe was representative for the area.

[6] The sea ice was in the late stages of melt, with a melt pond coverage of about 23%. Figure S2 shows an aerial photo of a region approximately 560 by 370 m, including most of the floe on which measurements were made along with some surrounding ice and open water. The photo has been corrected for vignetting and lens distortion. Using thresholds in the red and blue channels, each pixel was classified as white ice (bare, snow-free ice with a surface scattering layer of granular ice), open water, dark melt pond, or bright melt pond, also shown in Figure S2. Areas of submerged ice at floe edges are classified by the algorithm as ponds; while these areas would not normally be considered ponds, their optical effect is closer to that of ponds than to that of white ice or open water.

[7] Components of the energy budget that were continuously monitored include incoming and outgoing solar and terrestrial radiation, oceanic turbulent heat flux to the ice, and atmospheric turbulent sensible and latent heat fluxes to the ice. Transects were carried out on the surface with a sled-based system [*Hudson et al.*, 2012] and beneath the ice by divers to determine the spatial variability of the albedo and transmittance. From the transect data, the typical albedo and transmittance were determined separately for white ice

Additional supporting information may be found in the online version of this article.

[1]Norwegian Polar Institute, Tromsø, Norway.

Corresponding author: S. R. Hudson, Norwegian Polar Institute, Fram Centre, N-9296 Tromsø, Norway. (hudson@npolar.no)

0094-8276/13/10.1002/grl.50517

Table 1. The Mean Broadband Albedo and Transmittance of Each Surface Type [Values for Open Water are Assumed, e.g., *Perovich*, 2005], Along With the Area Fraction of Each Within the Focus Area (Figure S2)

	Albedo	Transmittance	Area Fraction
Open water	0.07	0.93	0.04
White ice	0.55	0.11	0.74
Bright pond	0.34	0.20	0.07
Dark pond	0.15	0.39	0.15

and bright and dark melt ponds. These values were used, together with the classified aerial photograph of the study area, to upscale the radiative properties of the ice in the region. Manual observations of ice thickness, freeboard, and melt pond depth were undertaken along the transmittance transects. Ship-based measurements of standard oceanographic and meteorological parameters are also available. For descriptions of the methods used during the campaign and analysis, see the supporting information.

3. Results

[8] The focus area for the following analysis is that shown in Figure S2. After masking out the ship, the area fraction of each surface type was determined, shown in Table 1, along with the mean albedo and transmittance for each type. Based on these values, the broadband albedo and transmittance of the focus area were 0.46 and 0.19, respectively. Excluding the open water fraction increases the albedo to 0.47 and reduces the transmittance to 0.16, indicating that the ice and ponds in the area absorbed about 37% of the solar energy incident on them.

[9] Time series of the observed fluxes during the period are shown in Figure 1, both individually and in total. The net longwave and net shortwave values plotted here are those observed at the radiometer site (over the edge of a small melt pond), with no upscaling and no special consideration of shortwave that was not absorbed by the ice, but transmitted to the water. Transmittance is not an issue for longwave fluxes, and spatial variability is minimal since the entire floe was at the melting point and under the same cloud cover. To account for spatial variability and transmittance in the shortwave, the values in Table 1 were used (with areas corrected to exclude open water), along with the time series of observed incident shortwave, to derive the time series of shortwave radiation absorbed by the ice. (By chance, the mean broadband albedo for the period at the site of the radiometer was 0.47, the same as that calculated for the floe. The difference between the two shortwave curves is therefore primarily illustrating the transmitted energy, with a smaller influence of the observed temporal variations in the albedo, not accounted for in the absorbed shortwave curve.)

[10] The thick black curve shows the time series of total energy absorbed by the ice and ponds, the sum of oceanic, latent, and sensible heat fluxes, net longwave, and shortwave absorbed by ice and ponds. Shortwave radiation was usually the largest source of energy to the ice, driving a clear diurnal cycle in the total energy absorption. Oceanic heat flux was also a significant source of energy at times, especially during the event on 30–31 July, when it climbed to over 70 W m^{-2}, coincident with increases in wind, ice drift, and ice-relative current speeds (Figure S3). During periods with incomplete or thinner cloud cover, longwave emission acted to cool the ice. Atmospheric turbulent fluxes were negligible throughout the period (the air temperature was within 2 K of freezing the entire time).

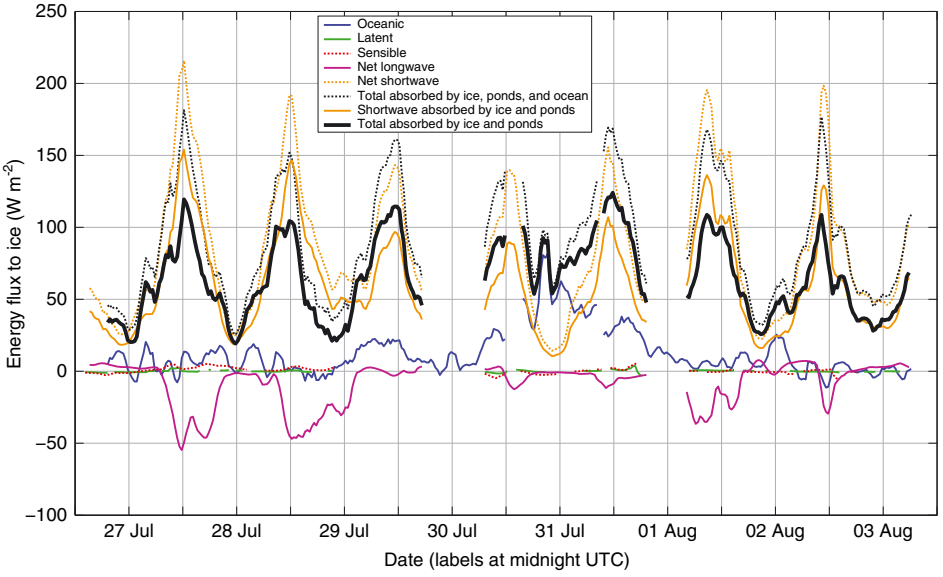

Figure 1. Time series of observed oceanic and atmospheric (sensible and latent) turbulent heat fluxes to the ice and net shortwave and longwave radiative fluxes. Also shown is the shortwave radiative flux absorbed by the ice and ponds in the ice-covered area shown in Figure S2 (using the observed incoming flux and the values from Table 1). Turbulent fluxes are positive when they are providing heat to the ice; negative longwave fluxes indicate the ice is losing more heat to surface emission than it is gaining from atmospheric emission. All fluxes have been smoothed with a 2 h running mean. Totals are calculated for both the amount of energy absorbed by the ice (thick line) and by the ice-ocean system. In calculating the totals, missing atmospheric turbulent fluxes were assumed to be zero.

Table 2. Average of the Observed Fluxes Absorbed by the Ice and Ponds (Mean Values of the Time Series Shown in Figure 1)[a]

	Average (W m^{-2})	Contribution (%)
Shortwave	60.2	92.9
Longwave	–9.0	–13.8
Oceanic	13.1	20.3
Sensible	0.4	0.6
Latent	0.1	0.1
Total absorbed	64.8	100
Transmitted shortwave	26.0	–

[a]The shortwave value excludes that which was reflected or transmitted. The values are also presented as relative contributions to the total energy absorbed by the ice and ponds during the period. The bottom line shows the solar energy transmitted through the ice and ponds to the underlying ocean water.

[11] On average, 60 W m^{-2} of shortwave radiation was absorbed by the ice and ponds, and 26 W m^{-2} was transmitted through ice and ponds to the ocean (direct absorption by open water areas is not included in either of these values). Oceanic heat fluxes averaged 13 W m^{-2} to the ice, while longwave radiation resulted in an average energy loss of 9 W m^{-2}. Averages and relative contributions for the period are summarized in Table 2.

[12] In total, during the 7.7 day period, the ice and ponds absorbed 43 MJ m^{-2}, enough to melt 14 cm of pure, solid ice. The observed ocean heat flux would provide 2 cm of bottom melt. The absorbed solar energy could melt 13 cm of ice, largely at the surface, but some of the energy was deposited internally and at the lower ice-ocean interface. The combined atmospheric and longwave fluxes help to offset the surface melt due to solar absorption, providing about 1 cm of potential surface freezing.

[13] Thickness measurements made every meter along a 32 m transect across a mix of white and ponded ice on 28 July and 2 August show an average loss of 17.2 cm of ice (21.1 cm averaged over ponded areas and 14.0 cm over white areas; no distinction between surface and bottom ablation). The surface along the 32 m profile was 50% white ice and 50% dark pond; using the resulting albedo and transmittance for this mixture of surface types to calculate the energy absorbed by the ice during the 5.5 days results in a potential melt of 10.8 cm of pure ice. The discrepancy between this calculated and the observed melt is likely due to a combination of the presence of salt in the ice and the fact that neither the top nor the bottom of the ice is solid (the top is a scattering layer, similar to snow, and the bottom is porous). Using a latent heat of fusion of 275 kJ kg^{-1}, corresponding to a salinity of 6 [*Stanton et al.*, 2012], and a density of 700 kg m^{-3} provides a calculated melt of 17.2 cm (19.6 cm for ponds and 14.8 cm for white ice). Similar agreement could be obtained with a higher latent heat and lower density.

4. Discussion

[14] In comparison to melting MYI, we find the albedo of bare white FYI is lower (0.55, compared to 0.6–0.7) [*Perovich*, 2005], and transmittances are higher for both white and ponded ice (0.11 and 0.33 area-weighted average of our light and dark ponds), compared to 0.07 and 0.26, [*Light et al.*, 2008, for a thickness of 0.8 m, using their equation (3) and Table 4 and the fraction of short and longwave fluxes in our mean incoming solar spectrum].

[15] At Surface Heat Budget of the Arctic Ocean (SHEBA), *Perovich* [2005] reported the aggregate scale albedo in late July to be 0.5–0.6, with aggregate scale transmittance around 0.15, both with about 5% open water and 20–25% pond coverage. In early August, an ice divergence event increased the open-water fraction at SHEBA to about 20%, decreasing the albedo to 0.40 and increasing the transmittance to 0.27. Figure 2 shows the resulting aggregate scale albedo and transmittance for a region as a function of pond and open-water fraction, based on the average ice and pond albedo and transmittance observed in this study (therefore relevant for ice of a similar thickness, 0.8 m on average). The pond fraction at SHEBA was similar to that in this study. With open water covering 5% of the area, the values derived here produce aggregate albedo and transmittance of 0.45 and 0.20, about 18% less reflective than in late July at SHEBA, and transmitting about 33% more energy to the ocean. These differences must be mostly attributable to the thinner ice studied here. At 20% open water, the values here are 0.38 and 0.33, for albedo and transmittance, respectively; again, less reflective and more transmissive but with less significant differences because of the importance of the open water area. This change illustrates the radiative importance of the thinning and other changes taking place in the Arctic ice cover.

[16] Compared to the FYI case presented by *Nicolaus et al.* [2012], our aggregate transmittance of 0.16 is somewhat greater than their value of 0.11, despite much greater pond coverage on their floe (42%). Their albedo (0.37) is considerably lower than ours (0.47), in line with the large pond coverage. Our derived pond and white ice transmittances (0.32 area-weighted pond average and 0.11 white) are considerably higher than those found by *Nicolaus et al.* [2012], 0.22 and 0.04. These transmittance differences are

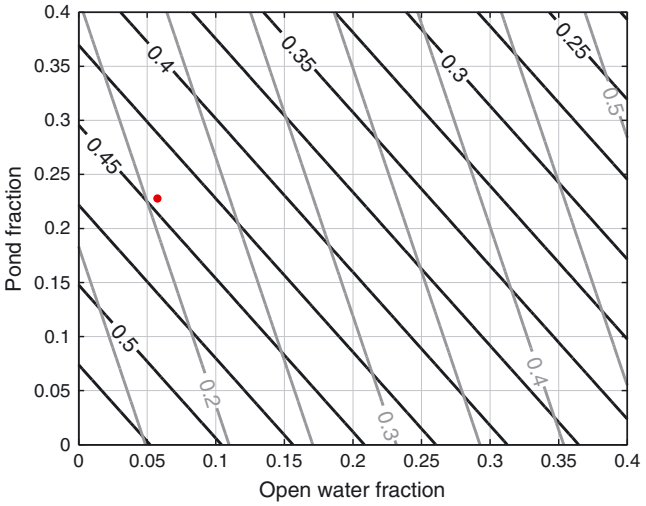

Figure 2. Based on the typical observed albedo and transmittance of the surface types on the investigated floe, the aggregate scale albedo (black) and transmittance (gray) are contoured for a range of pond fractions and open water fractions. The distribution of total pond area into bright and dark ponds was held constant at the observed value; 67.5% of all ponds were dark. The red dot shows the observed pond fraction and open water fraction for the photo making up the main study area (Figure S2).

again due to ice thickness differences between the two studies (1.3 m, compared to 0.8 m here), and possibly also to larger solar zenith angles later in the season.

[17] In the data set presented here, oceanic turbulent heat flux provided, on average, 13 W m^{-2} of energy to the ice, 20% of the total, and at times, it became the most significant heat source, climbing to over 70 W m^{-2}. The largest heat fluxes were measured during a relatively long period (about 30 h on 30–31 July) with strong winds (8–12 m s^{-1}, see Figure S3). Similar wind speeds and somewhat elevated heat fluxes (about 20 W m^{-2}) were also recorded on 29 July, in an event lasting about 18 h. While conductivity-temperature-depth data show some deepening of the main pycnocline (not shown) during this first event, and under-ice relative current speeds were comparable during both events (Figure S3), it appears that more mixing energy was dissipated deeper down during the following, longer strong wind episode, allowing for larger sustained upward heat fluxes from the subsurface heat reservoir. There was also more heat available (greater difference between local freezing point and water temperature) in this subsurface layer during the second wind event (not shown), possibly as a result of the change in wind direction and ice drift which forced the pack ice to diverge, thus allowing for a larger lead fraction and greater solar absorption in the ocean in the second half of the drift.

[18] Our average value of ocean heat flux compares well with earlier observations of oceanic heat flux resulting from summertime solar heating of the upper ocean [see *McPhee et al*., 2003, and references therein]. *Stanton et al.* [2012] reported average ocean heat fluxes of 15 W m^{-2} in the transpolar drift in mid-July to late August, the period of maximum fluxes in their 2002–2010 data set. Our peak ocean heat fluxes are at the upper end of those observed by *Stanton et al.* [2012] from 2008 to 2010 and significantly larger than those observed by them in years before 2007. *Perovich and Elder* [2002] inferred weekly oceanic heat fluxes during SHEBA, giving a range of 0–30 W m^{-2}, with an increase from spring to summer attributed to solar heating. *Shaw et al.* [2009] presented ocean-ice heat fluxes at SHEBA that average 14 W m^{-2} in August–September 1998, while the drift was in deep water. *Sirevaag et al.* [2011] reported lower average oceanic heat fluxes of 1.2 W m^{-2} in the Amundsen basin in late August for a thicker snow-covered ice pack with much less solar radiation (2.6 W m^{-2}) reaching the ocean; the ratio of ocean heat flux to solar transmittance was the same during their study and the one presented here.

[19] Our drift stayed in the deep basin (depths greater than 3000 m), and we saw no evidence that ocean heat fluxes were significantly enhanced by mixing of warmer Atlantic water, as was observed by *McPhee et al.* [2003] over the shallower Yermak Plateau, west of our location. Yet our maximum ocean heat fluxes reached similar peak values. Wind speeds appear to have been typical for the region in summer (see supporting information). We surmise that the larger oceanic heat flux was supported by the increased solar transmittance through this thinner ice pack, which resulted in accumulation of heat in a subsurface layer, evidenced by a near-surface temperature maximum (NSTM) 0.3–0.4 K above local freezing at 10–30 m depth (e.g., Figure S4), much higher than those observed by *McPhee et al.* [2003] for summer conditions in the deep basin (< 0.15 K). During our observations, the oceanic heat flux was about half of the solar flux penetrating the ice (which was about the same as the calculated solar flux into open water in the transpolar drift study by *Stanton et al.* [2012], without including radiation entering open water here), leaving another 13 W m^{-2} of solar heating being trapped at depth due to surface stratification from ice melt and the subsequent formation of a NSTM. The upper level of the NSTM was closely associated with the pycnocline (Figure S4), as described by *Jackson et al.* [2010] in the Canada Basin.

[20] Release of this heat to the surface later in the autumn or during strong wind events [*Zhang et al.*, 2013] could significantly extend the effect of the increase in solar radiation absorbed by the system. The excess heat (above local freezing) contained in just the 30 m layer from 10 to 40 m below our floe was enough to melt about 12 cm of ice, or to delay freeze-up by about 9 days, assuming a late summer-early autumn cooling rate of 50 W m^{-2}. (50 is approximately the longwave cooling rate for a surface at freezing below a clear atmosphere, see the peak longwave cooling rates in Figure 1. Since there is usually some solar energy remaining when freeze-up begins and no local source of very cold air, and since cloud cover reduces the longwave cooling, this seems a generous estimate of the cooling rate at the onset of freeze-up, and therefore a conservative estimate on the delay.)

5. Conclusion

[21] We collected the first simultaneous observations of all components of the energy budget of thin, melting first-year sea ice in the high Arctic. From these, we found that in late summer, the absorption of sunlight was the largest source of energy to the ice, often even at midnight. However, the oceanic heat flux was comparable to nighttime solar absorption and sometimes significantly exceeded it during wind events. Atmospheric heat fluxes were not important during the period. The thinner ice cover now extending over the Arctic allows more solar radiation to penetrate it and warm the ocean. While about half of this heat seems to be returned to the ice over short time periods, the rest results in a near-surface temperature maximum significantly above local freezing. Most of this trapped heat is likely mixed to the surface at some point, either resulting in additional rapid melt, or in a delayed freeze-up.

[22] *Maslanik et al.* [2011] showed that multiyear ice extent in the Arctic has decreased from about 4.5×10^6 km^2 in the 1980s (average of March and September extents) to about 2.0×10^6 km^2 in 2008 (updated data at http://nsidc.org/arcticseaicenews/2013/04/ show 2013 is similar to 2008, after an intervening increase). Most of this area remains ice-covered in July, but with first-year ice. If the aggregate-scale albedo and transmittance changes between SHEBA and this study apply over the whole area for the 4 week period from early July to early August, then assuming our observed solar radiation conditions are typical for the period and area, the change from multiyear to first-year ice over this region results in an additional solar input to the ice and ocean of 1×10^{20} J, enough energy to melt 315 km^3 of ice, or nearly 13 cm over the entire affected area. Half of this energy is due to increased absorption in the ice and ponds, the rest to increased transmittance. Using the aggregate properties of FYI derived by *Nicolaus et al.* [2012]

would give an even larger result (with a very different partitioning between ice-pond and ocean absorption), as would considering solar flux directly into areas that have become ice free. This result clearly illustrates the importance of the Arctic regime shift and the feedbacks that play a role long before the ice disappears completely.

[23] **Acknowledgments.** We thank the crew of R/V *Lance* and the other scientists and engineers on board, in particular Jens Ehn, for their assistance in carrying out the measurements. We are very grateful to Haakon Hop, Rupert Krapp, Peter Leopold, Michael Tessmann, and Jago Wallenschus for carrying out the diving to measure radiation below the ice. We also thank two anonymous reviewers, Marcel Nicolaus, and Editor Julienne Stroeve for helpful comments that improved the paper. Funding was provided by the Centre for Ice, Climate and Ecosystems (ICE) at the Norwegian Polar Institute and by the Norwegian Research Council, through the FRINAT program (grant 197236/V30). This work was also supported by ACCESS, a European Project within the Ocean of Tomorrow call of the European Commission Seventh Framework Programme, grant 265863.

[24] The Editor thanks two anonymous reviewers for their assistance in evaluating this paper.

References

Comiso, J. C. (2012), Large decadal decline of the Arctic multiyear ice cover, *J. Climate*, *25*, 1176–1193, doi:10.1175/JCLI-D-11-00113.1.

Frey, K. E., D. K. Perovich, and B. Light (2011), The spatial distribution of solar radiation under a melting Arctic sea ice cover, *Geophys. Res. Lett.*, *38*, L22501, doi:10.1029/2011GL049421.

Giles, K. A., S. W. Laxon, and A. L. Ridout (2008), Circumpolar thinning of Arctic sea ice following the 2007 record ice extent minimum, *Geophys. Res. Lett.*, *35*, L22502, doi:10.1029/2008GL035710.

Haas, C. A., S. Hendricks, L. Rabenstein, J. Etienne, and I. Rigor (2008), Reduced ice thickness in Arctic Transpolar Drift favors rapid ice retreat, *Geophys. Res. Lett.*, *35*, L17501, doi:10.1029/2008GL034457.

Hudson, S. R., M. A. Granskog, T. I. Karlsen, and K. Fossan (2012), An integrated platform for observing the radiation budget of sea ice at different spatial scales, *Cold Reg. Sci. Technol.*, *82*, 14–20, doi:10.1016/j.coldregions.2012.05.002.

Jackson, J. M., E. C. Carmack, F. A. McLaughlin, S. E. Allen, and R. G. Ingram (2010), Identification, characterization, and change of the near-surface temperature maximum in the Canada Basin, 1993–2008, *J. Geophys. Res.*, *115*, C05021, doi:10.1029/2009JC005265.

Laxon, S. W., et al. (2013), Cryosat-2 estimates of Arctic sea ice thickness and volume, *Geophys. Res. Lett.*, *40*, 732–737, doi:10.1002/grl.50193.

Light, B., T. C. Grenfell, and D. K. Perovich (2008), Transmission and absorption of solar radiation by Arctic sea ice during the melt season, *J. Geophys. Res.*, *113*, C03023, doi:10.1029/2006JC003977.

Markus, T., J. C. Stroeve, and J. Miller (2009), Recent changes in Arctic sea ice melt onset, freezeup, and melt season length, *J. Geophys. Res.*, *114*, C12024, doi:10.1029/2009JC005436.

Maslanik, J., J. Stroeve, C. Fowler, and W. Emery (2011), Distribution and trends in Arctic sea ice age through spring 2011, *Geophys. Res. Lett.*, *38*, L13502, doi:10.1029/2011GL047735.

McPhee, M. G., T. Kikuchi, J. H. Morison, and T. P. Stanton (2003), Ocean-to-ice heat flux at the North Pole environmental observatory, *Geophys. Res. Lett.*, *30*, 2274, doi:10.1029/2003GL018580.

Nicolaus, M., C. Katlein, J. Maslanik, and S. Hendricks (2012), Changes in Arctic sea ice result in increasing light transmittance and absorption, *Geophys. Res. Lett.*, *39*, L24501, doi:10.1029/2012GL053738.

Perovich, D. K. (2005), On the aggregate-scale partitioning of solar radiation in Arctic sea ice during the Surface Heat Budget of the Arctic Ocean (SHEBA) field experiment, *J. Geophys. Res.*, *110*, C03002, doi:10.1029/2004JC002512.

Perovich, D. K., and B. Elder (2002), Estimates of ocean heat flux at SHEBA, *Geophys. Res. Lett.*, *29*, 1344, doi:10.1029/2001GL01471.

Perovich, D. K., and C. Polashenski (2012), Albedo evolution of seasonal Arctic sea ice, *Geophys. Res. Lett.*, *39*, L08501, doi:10.1029/2012GL051432.

Polashenski, C., D. Perovich, and Z. Courville (2012), The mechanisms of sea ice melt pond formation and evolution, *J. Geophys. Res.*, *117*, C01001, doi:10.1029/2011JC007231.

Shaw, W. J., T. P. Stanton, M. G. McPhee, J. H. Morison, and D. G. Martinson (2009), Role of the upper ocean in the energy budget of Arctic sea ice during SHEBA, *J. Geophys. Res.*, *114*, C06012, doi:10.1029/2008JC004991.

Sirevaag, A., S. de la Rosa, I. Fer, M. Nicolaus, M. Tjernström, and M. G. McPhee (2011), Mixing, heat fluxes and heat content evolution of the Arctic Ocean mixed layer, *Ocean Sci.*, *7*, 335–349, doi:10.5194/os-7-335-2011.

Stanton, T. P., W. J. Shaw, and J. K. Hutchings (2012), Observational study of relationships between incoming radiation, open water fraction, and ocean-to-ice heat flux in the Transpolar Drift: 2002–2010, *J. Geophys. Res.*, *117*, C07005, doi:10.1029/2011JC007871.

Stroeve, J. C., M. C. Serreze, M. M. Holland, J. E. Kay, J. Malanik, and A. P. Barrett (2012), The Arctic's rapidly shrinking sea ice cover: A research synthesis, *Clim. Change*, *110*, 1005–1027, doi:10.1007/s10584-011-0101-1.

Wadhams, P., and N. Toberg (2012), Changing characteristics of Arctic pressure ridges, *Polar Sci.*, *6*, 71–77, doi:10.1016/j.polar.2012.03.002.

Zhang, J., R. Lindsay, A. Schweiger, and M. Steele (2013), The impact of an intense summer cyclone on 2012 Arctic sea ice retreat, *Geophys. Res. Lett.*, *40*, doi:10.1002/grl.50190.